Journal of Controlled Release 343 (2022) 338–346

Contents lists available at ScienceDirect

Journal of Controlled Release

journal homepage: www.elsevier.com/locate/jconrel

Tuning the size of all-HPMA polymeric micelles fabricated by solvent extraction

Yan Wang [a], Dominique M.E. Thies-Weesie [b], Esmeralda D.C. Bosman [a], Mies J. van Steenbergen [a], Joep van den Dikkenberg [a], Yang Shi [c], Twan Lammers [c], Cornelus F. van Nostrum [a], Wim E. Hennink [a,*]

[a] Department of Pharmaceutics, Utrecht Institute for Pharmaceutical Sciences, Utrecht University, Universiteitsweg 99, 3508 TB Utrecht, the Netherlands
[b] Department of Physical and Colloid Chemistry, Debye Institute for Nanomaterials Science, Utrecht University, Padualaan 8, 3584 CH Utrecht, the Netherlands
[c] Department of Nanomedicine and Theranostics, Institute for Experimental Molecular Imaging, RWTH Aachen University Clinic, Forckenbecktrasse 55, 52074 Aachen, Germany

A B S T R A C T

The size of polymeric micelles crucially affects their tumor accumulation, penetration and antitumor efficacy. In the present study, micelles were formed based on amphiphilic poly(*N*-2-hydroxypropyl methacrylamide)-*block*-poly(*N*-2-benzoyloxypropyl methacrylamide) (p(HPMAm)-b-p(HPMAm-Bz)) via the solvent extraction method, and factors impacting micelle size were systematically studied, including the molecular weight of the polymers, homopolymer content, and processing methods (i.e., batch process versus continuous microfluidics). The formation of core-shell structured micelles was demonstrated by light scattering, sedimentation velocity and electron microscopy analysis. Micellar size and aggregation number increased with decreasing the molecular weight ratio of the hydrophilic/hydrophobic block. The presence of hydrophobic p(HPMAm-Bz) homopolymer and high copolymer concentration increased micelle size, while the presence of hydrophilic p(HPMAm) homopolymer did not affect micellar size. Regarding processing conditions, it was found that the use of tetrahydrofuran and acetone as solvents for the polymers resulted in larger micelles, likely due to their relatively high water-solvent interaction parameters as compared to other solvents tested, i.e., dimethylformamide, dimethylacetamide, and dimethyl sulfoxide. Among the latter, only dimethylformamide led to micelles with a narrow polydispersity. Addition of dimethylformamide to an aqueous solvent and faster mixing of two solvents using microfluidics favored the formation of smaller micelles. In conclusion, our results show that the size of all-HPMA polymeric micelles can be easily tailored from 40 to 120 nm by varying the formulation properties and processing parameters.

1. Introduction

In aqueous solution, amphiphilic block copolymers self-assemble into polymeric micelles composed of hydrophobic core – hydrophilic shell architectures which can be used for solubilization and targeted delivery of cytostatic drugs [1–5]. Their hydrophobic core is able to accommodate poorly water-soluble drugs via either physical entrapment or chemical attachment, while their hydrophilic shell ensures colloidal stability [6–8]. Upon intravenous administration, the nano-size of polymeric micelles (usually 10–100 nm) and their hydrophilic shell contribute to prolonged blood circulation by avoiding protein adsorption and uptake by the mononuclear phagocyte system (MPS) [9,10]. This prolonged circulation leads to increased accumulation of drug payloads in cancerous and inflamed tissues due to increased vascular permeability and impaired lymphatic drainage, known as the enhanced permeability and retention (EPR) effect [11,12].

The efficacy of nanoparticulate drug delivery systems is affected by many physical and chemical characteristics, including size, shape, and surface properties (i.e., surface charge and the presence of targeting ligands) [13–17]. Among these factors, the size of polymeric micelles and size distribution play a critical role regarding circulation, tumor disposition and penetration, and cellular uptake [18]. In recent years, the effect of size of nanoparticles on their efficacy of cancer treatment have been extensively studied. For example, Tang et al. prepared micelles based on polyethylene glycol (PEG) and 10-OH methacrylate ester of 7-ethyl-10-hydroxyl-camptothecin (HEMASN38). The authors showed that 100 nm PEG-b-P(HEMASN38) micelles had prolonged blood circulation and improved tumor accumulation as compared to 30 nm size micelles [19]. However, these 30 nm micelles showed better tumor penetration. Kataoka et al. reported that PEG-b-poly(glutamic acid) micelles with average size of 30, 50, 70 and 100 nm penetrated highly permeable tumors, whereas only micelles of 30 nm were able to penetrate poorly permeable pancreatic tumors and showed antitumor effects [20]. On the contrary, Liang et al. found that ultrasmall tiopronin-coated

* Corresponding author.
E-mail address: W.E.Hennink@uu.nl (W.E. Hennink).

https://doi.org/10.1016/j.jconrel.2022.01.042
Received 22 November 2021; Received in revised form 23 January 2022; Accepted 24 January 2022
Available online 29 January 2022

gold nanoparticles (2 and 6 nm) had longer blood circulation times than 15 nm gold nanoparticles [21]. However, ultrasmall nanodrugs may undergo rapid renal clearance, resulting in inadequate tumor accumulation [22]. Overall, the optimal size of polymeric micelles should be large enough for long circulation time and high tumor accumulation (> 5.5 nm) [23], but small enough for good tumor penetration (< 100 nm) [24].

Recently, we reported the synthesis of amphiphilic poly(*N*-2-hydroxypropyl methacrylamide)-*block*-poly(*N*-2-benzoyloxypropyl methacrylamide) (p(HPMAm)-b-p(HPMAm-Bz)) with a molecular weight ranging from 8 to 24 kDa via reversible addition–fragmentation chain-transfer (RAFT) polymerization [25]. Micelles based on p(HPMAm)-b-p(HPMAm-Bz) with a molecular weight of 22.1 kDa showed good colloidal stability and drug loading. In the present study, a systematic evaluation was performed to investigate the parameters that affect the size of p(HPMAm)-b-p(HPMAm-Bz) micelles formed using batch preparation and continuous microfluidics. These include: (1) formulation variables, namely the type of solvent for the block copolymer, polymer concentration, homopolymer content, and the molecular weight ratio of the hydrophobic/hydrophilic block, as well as (2) processing variables, namely order of addition of solvent and non-solvent (water), volume ratio and mixing time of the organic phase and aqueous medium. The formed micelles were characterized using various techniques, including asymmetric flow field-flow fractionation coupled with multi-angle light scattering and dynamic light scattering, ultracentrifugation and electronic microscopy. The purpose was to find a highly reproducible method for formation of all-HPMAm based micelles with tunable size.

2. Experiments

2.1. Materials

Dimethylformamide (DMF), tetrahydrofuran (THF), dimethylacetamide (DMAc), dimethyl sulfoxide (DMSO), and acetone were purchased from Biosolve Ltd. (Valkenswaard, the Netherlands) and used as received. Syringe filters with 0.45 μm regenerate cellulose (RC) membrane were purchased from Phenomenex (Utrecht, the Netherlands), while 0.2 μm polytetrafluoroethylene (PTFE) membrane and 0.2 μm RC membrane filters were ordered from Roth (Karlsruhe, Germany). Bovine serum albumin was purchased from Sigma-Aldrich (Zwijndrecht, the Netherlands). Poly(*N*-2-hydroxypropyl methacrylamide) (p(HPMAm)), poly(*N*-2-benzoyloxypropyl methacrylamide) (p(HPMAm-Bz)), and p(HPMAm)-b-p(HPMAm-Bz) which were synthesized and characterized as previously reported are shown in Scheme S1 & Table S1 [25].

2.2. Preparation of p(HPMAm)-b-p(HPMAm-Bz) micelles

p(HPMAm)-b-p(HPMAm-Bz) micelles were prepared by solvent extraction method. In detail, 1 mL DMF solution of 20 mg p(HPMAm)-b-p(HPMAm-Bz) copolymer was pipetted into 1 mL of Milli-Q water while stirring for 1 min. To remove DMF, the mixture was transferred into a Spectra/Por dialysis membrane with a molecular weight cutoff of 6–8 kDa which was subsequently sealed. Dialysis was carried out for 24 h against Milli-Q water which was changed at 2nd, 5th, and 13th h. Next, the micellar dispersion was filtered through 0.45 μm RC membrane filter.

2.2.1. Effect of solvent composition on the micellar size

THF, acetone, DMAc, DMF, and DMSO were used to investigate the effect of the type of organic solvent on the size of p(HPMAm)-b-p(HPMAm-Bz) micelles. In short, p(HPMAm)$_{7.1k}$-b-p(HPMAm-Bz)$_{15.0k}$ copolymer (20 mg) was dissolved in 1 mL of the organic solvents mentioned and the obtained solution was pipetted into 1 mL of Milli-Q water while stirring for 1 min. THF and acetone were removed by evaporation overnight at room temperature, while DMAc, DMF, and DMSO were removed by dialysis, resulting in the formation of micelles.

The effect of the composition of the aqueous solution on the size of the micelles was also investigated. Water, 0.9% NaCl solution, and phosphate-buffered saline (PBS, pH 7.4, containing 11.9 mM phosphate, 137 mM sodium chloride, and 2.7 mM potassium chloride) were used as aqueous medium. 1 mL DMF solution of 20 mg of p(HPMAm)$_{7.1k}$-b-p(HPMAm-Bz)$_{15.0k}$ copolymer was pipetted into 1 mL of Milli-Q water, 0.9% NaCl solution, or PBS while stirring for 1 min, followed by dialysis and filtration through 0.45 μm RC membrane filter.

2.2.2. Effect of the polymer concentration in DMF on the micellar size

The effect of polymer concentration in DMF on the size of p(HPMAm)-b-p(HPMAm-Bz) micelles was investigated. Briefly, 1 mL DMF solution of different amounts of p(HPMAm)$_{7.1k}$-b-p(HPMAm-Bz)$_{15.0k}$ copolymer (5, 10, 20, 30, and 40 mg) was pipetted into 1 mL of Milli-Q water while stirring for 1 min, followed by dialysis and filtration through 0.45 μm RC membrane filter.

2.2.3. Effect of organic/aqueous solvent ratio and the order of solvent addition on the micellar size

To investigate the effect of organic to aqueous solvent ratio and the order of solvent addition on the size of the formed p(HPMAm)-b-p(HPMAm-Bz) micelles, experiments were carried out where the volume ratios of the polymer solution in DMF to water were 1:1 and 0.3:1, and the addition order of two solvents (DMF to water or water to DMF) was changed. In brief, p(HPMAm)$_{7.1k}$-b-p(HPMAm-Bz)$_{15.0k}$ copolymer (20 mg) was dissolved in DMF (0.3 or 1.0 mL), and the obtained solution was either pipetted into Milli-Q water or water was added to this solution while stirring for 1 min, followed by dialysis and filtration through 0.45 μm RC membrane filter. The critical overlap concentration (C*) of the block copolymer p(HPMAm)-b-p(HPMAm-Bz) (total molecular weight 22 kDa) in DMF was calculated using the experimentally determined intrinsic viscosity [ŋ] (C* = 1/[ŋ]) [26]. The flow times of DMF and solutions of this polymer (10, 21 and 28 mg/mL) were measured as the average of three readings with an accuracy of ±0.2 s. The intrinsic viscosity was calculated by extrapolating the plot of the reduced viscosity η_{sp}/c versus polymer concentration c to c = 0 using the classical Huggins Eq. [27].

2.2.4. Effect of mixing time of organic and aqueous solvent on the micellar size

The effect of mixing time of organic and aqueous solvent on the size of the formed p(HPMAm)-b-p(HPMAm-Bz) micelles was investigated using Dolomite microfluidics (Dolomite Center Ltd., Royston, UK). In detail, a solution of block copolymer in DMF (20 mg/mL, p(HPMAm)$_{7.1k}$-b-p(HPMAm-Bz)$_{15.0k}$, p(HPMAm)$_{7.1k}$-b-p(HPMAm-Bz)$_{9.1k}$, or p(HPMAm)$_{4.9k}$-b-p(HPMAm-Bz)$_{11.3k}$) was filtered with a 0.2 μm PTFE syringe filter, and Milli-Q water was filtered with a 0.2 μm RC syringe filter. Both solvents were placed in chambers which were connected to pumps. These pumps were connected to a Dolomite hydrophilic micromixer chip (Part No. 3200401) via a PTFE tubing. The polymer solution and Milli-Q water were mixed at a 1:1 volume ratio at different total flow rates (Q_{tot}, 100, 200, 350, 500, 1600, and 3000 μL/min) corresponding to varying mixing times (τ_M, 1571, 635, 306, 192, 42, and 18 ms) which were calculated based on data supplied by the manufacturer (Fig. S2). Two mL of the different micellar dispersions were collected after the mixture reached a steady-state flow. DMF was subsequently removed by dialysis against water.

2.2.5. Effect of the presence of free p(HPMAm) and p(HPMAm-Bz) homopolymer on the micellar size

The effect of free p(HPMAm) and p(HPMAm-Bz) homopolymer on the size of the formed p(HPMAm)-b-p(HPMAm-Bz) micelles was investigated. In short, 20 mg of p(HPMAm)$_{7.1k}$-b-p(HPMAm-Bz)$_{15.0k}$ copolymer and 0, 1, 2, 5, and 10 mg of p(HPMAm)$_{7.1k}$ or p(HPMAm-Bz)$_{14.6k}$ were dissolved in 1 mL of DMF corresponding to weight fractions of 0, 5,

9, 20, and 33 wt% of the homopolymer, respectively. These solutions were mixed with 1 mL water and subsequently, DMF was removed by dialysis. Finally, the micellar dispersions were filtered through 0.45 μm RC membrane filter.

2.2.6. Effect of hydrophilic/hydrophobic molecular weight of copolymers on the micellar size

The effect of the hydrophilic/hydrophobic molecular weight of the block copolymers on the size of the formed micelles was investigated. Polymers with different hydrophilic and hydrophobic lengths at a total molecular weight of 8–24 kDa (Table S1) were used to prepare micelles. Briefly, p(HPMAm)-b-p(HPMAm-Bz) copolymer (20 mg) was dissolved in 1 mL DMF and the obtained solution was pipetted into 1 mL of Milli-Q water while stirring for 1 min, followed by dialysis and filtration through 0.45 μm RC membrane filter.

2.3. Characterization of p(HPMAm)-b-p(HPMAm-Bz) micelles

2.3.1. ^{1}H NMR spectroscopy

The residual organic solvent content of the micellar dispersion was measured by ^{1}H NMR analysis using a Bruker 600 MHz spectrometer (Bruker Corp., Massachusetts, USA) as described previously [28]. 200 μL of micelle dispersion was mixed with 400 μL of D_2O (containing 10 mg/mL sodium acetate as an internal standard), and the amount of residual organic solvent was calculated by comparing the integral of THF (3.60 ppm), acetone (2.22 ppm), DMAc (2.08 ppm), DMF (7.92 ppm), and DMSO (2.71 ppm) to that of sodium acetate (CH_3 at 1.76 ppm).

2.3.2. Thermo gravimetric analysis (TGA)

The polymer concentration in the different micellar dispersions was determined by thermo gravimetric analysis (TGA) using a TA instrument Q50 (Waters Corp., Delaware, USA). The analysis was performed by introducing 50 μL of dialyzed micelle dispersion into a tared aluminum pan, followed by heating from 20 to 120 °C at a heating rate of 20 °C/min with an isothermal hold time of 100 min. The weight of polymer residual was recorded over time. A sample of dry polymer, analyzed for comparison, displayed no mass loss indicating the stability of p(HPMAm)-b-p(HPMAm-Bz) polymers up to at least 120 °C.

2.3.3. Dynamic light scattering (DLS)

The size and size distribution of the formed p(HPMAm)-b-p(HPMAm-Bz) micelles were determined by dynamic light scattering (DLS) at 25 °C after 10-fold dilution in water using a Zetasizer Nano S at a fixed angle of 173° (Malvern Instruments Ltd., Malvern, UK). The size of micelles was also determined after addition of 1 mL of 1.8% NaCl solution or twice concentrated PBS (pH 7.4, containing 23.8 mM phosphate, 274 mM sodium chloride, and 5.4 mM potassium chloride) to 1 mL of micellar dispersions prepared in water. The *Z*-average diameter (Z_{ave}) and polydispersity index (PDI) were calculated by the Zetasizer software v.7.13.

2.3.4. Asymmetric flow field-flow fractionation and multi-angle light scattering (AF4-MALS)

The radius of gyration (R_g), the radius of hydration (R_h), and the molecular weight of different micelles ($M_{w,\ mic}$) were determined by asymmetric flow field-flow fractionation (AF4) measurements using a Postnova AF2000 system (Postnova Analytics, Landsberg, Germany) equipped with a degasser, isocratic pumps, auto sampler, and fraction collector. A Frit-inlet channel was equipped with a ceramic frit, a 350 μm spacer, and a regenerated cellulose membrane with a molecular weight cut-off of 10 kDa and kept at a temperature of 25 °C. The AF4 system was coupled to a refractive index (RI) detector, a multi-angle light scattering (MALS) detector and a DLS system (Malvern Instruments Ltd., Malvern, UK). Bovine serum albumin dissolved in 0.9% NaCl at a concentration of 5 mg/mL was used for calibration. PBS (pH 7.4, containing 11.9 mM phosphate, 137 mM sodium chloride, and 2.7 mM potassium chloride) was used as eluent. The micellar dispersions in water were diluted in PBS to a final concentration of 1.2 mg/mL. A 20 μL of sample was injected into the system and the detector flow was kept at 0.5 mL/min. The crossflow rate was initially 1.5 mL/min and then decreased exponentially in 70 min to 0.0 mL/min. After completion of the elution program, crossflow rate was maintained at 0.0 mL/min for at least 5 min to ensure complete elution of largest particles. Data acquisition and processing were executed with an AF2000 control software v.2.1.0.5, from which R_g, R_h, and $M_{w,\ mic}$ of micelles were calculated using a random coil fitting model [29]. The refractive index increment of the polymer (dn/dc), which is required for the determination of the molecular weight, was measured in water by injection of 20 μL of micellar dispersion (concentration accurately determined using TGA) into the AF4 channel without crossflow using a detector flow rate of 0.5 mL/min over 10 min.

2.3.5. Ultracentrifugation

The molecular weight of two selected micelles based on p(HPMAm)$_{3.0k}$-b-p(HPMAm-Bz)$_{15.6k}$ and p(HPMAm)$_{4.9k}$-b-p(HPMAm-Bz)$_{11.3k}$ was determined by sedimentation velocity experiments using a Proteomelab XL-I analytical ultracentrifuge (Beckman Coulter Inc., California, USA) equipped with absorbance optics. Diluted micelle dispersions were centrifuged in 3 mm pathlength double-sector Epon centerpieces with quartz centerpieces in an An-60 Ti rotor; the reference sector was filled with Milli-Q water. The micelle concentration was accurately determined using TGA and it turned out to be 0.54 mg/mL for p(HPMAm)$_{3.0k}$-b-p(HPMAm-Bz)$_{15.6k}$ and 1.21 mg/mL for p(HPMAm)$_{4.9k}$-b-p(HPMAm-Bz)$_{11.3k}$, respectively. The samples were centrifuged at 20 °C at a rotor speed of 8,000 rpm (5152 g) for p(HPMAm)$_{3.0k}$-b-p(HPMAm-Bz)$_{15.6k}$ micelles and 15,000 rpm (18,112 g) for p(HPMAm)$_{4.9k}$-b-p(HPMAm-Bz)$_{11.3k}$, respectively. Changes in solute micelle concentrations were detected by 200–300 absorbance scans measured at 272 nm. Analysis and fitting of the data was performed using the program Sedfit v.16.1c. A continuous c(M) distribution model was fitted to the data [30]; the distribution was integrated to calculate the average molecular weight of micelles ($M_{w,\ mic}$). From the known molecular weight of one polymer chain, the aggregation number of polymers per micelle was calculated to obtain N_{agg}. Partial specific volume of the micelles ($\bar{\nu}$), required for the determination of the molecular weight $M_{w,\ mic}$, was calculated from density measurements of series of diluted micelles (concentration ranging from 0.8 to 5.5 mg/ml at 20.00 ± 0.01 °C using a high-precision density meter DMA5000 (Anton Paar GmbH, Graz, Austria) according to the following equation:

$$\rho = \rho_0 + (1 - \bar{\nu}\,\rho_0)c$$

where ρ is density of micelle dispersion, ρ_0 is density of water, and c is concentration of micelles.

2.3.6. Electron microscopy (EM) analysis

The morphology of p(HPMAm)$_{7.1k}$-b-p(HPMAm-Bz)$_{15.0k}$ micelles formed under different conditions was visualized by transmission electron microscope (TEM) using a JEOL JEM-1400 TEM instrument (JEOL Ltd., Tokyo, Japan) operated with 100 kv acceleration voltages and 40 μA beam current. Samples were prepared by drying a drop of micellar dispersions in water (5 μL, 1 mg/mL) on a 400-mesh copper grid with lacey carbon support (Electron Microscopy Sciences, Pennsylvania, USA), subsequently stained with uranyl acetate solution (2%, *w/v*) before TEM observation.

The morphology of selected micelles based on p(HPMAm)$_{3.0k}$-b-p(HPMAm-Bz)$_{15.6k}$ and p(HPMAm)$_{4.9k}$-b-p(HPMAm-Bz)$_{11.3k}$ was investigated by cryogenic TEM (Cryo-TEM) using a Philips Tecnai 20 (FEI/Philips Electrons Optics, Eindhoven, the Netherlands). Samples for Cryo-TEM were prepared by glow-discharging the 300-mesh copper grid with lacey carbon support (Electron Microscopy Sciences, Pennsylvania, USA) in a Cressington 208 carbon coater for 40 s. Then, 3 μL of micellar

dispersion was pipetted onto the grid and blotted for 3–4 s in a fully automated vitrification robot (Vitrobot MARK IV, Thermo Fisher/FEI, Eindhoven, the Netherlands) at room temperature and 100% humidity. The grid was subsequently plunged into liquid ethane and stored under liquid nitrogen. Cryo-TEM images were recorded using a Gatan 626 holder (Gatan, California, USA). Brightness and contrast corrections of the acquired images were performed using the ImageJ software.

3. Results and discussion

3.1. Effect of solvent and anti-solvent on the size of all-p(HPMAm) micelles

Various organic solvents were used to investigate the effect on the size of p(HPMAm)$_{7.1k}$-b-p(HPMAm-Bz)$_{15.0k}$ micelles prepared by solvent extraction. ^{1}H NMR analysis showed that the amount of THF and acetone of the micellar dispersions after solvent evaporation for 24 h was far below the recommended limit of residual solvent for humanized use according to ICH guidelines (<720 and 5000 ppm, respectively, Table S2) [31]. However, these micellar dispersions also contained up to 2000 ppm of DMAc the solvent used for polymer synthesis that was not removed by evaporation due to its high boiling point (165 °C) (Fig. S1). Importantly, the residual concentration of the non-volatile solvent DMAc, DMF and DMSO was far below the recommended limit (<1090, 880, and 5000 ppm, respectively, Table S2) after dialysis for 24 h. Fig. 1A shows that the Z_{ave} of the different micelles varied from 61 ± 1 to 113 ± 7 nm (PDI < 0.2) with the smallest and largest micelles obtained using DMAc and THF, respectively. Both DLS and TEM analyses showed that micelles obtained using DMAc, DMF, and DMSO exhibited similar sizes (60–70 nm by DLS and 30–50 nm by TEM) (Fig. 1A).

Solvent extraction, also referred to as nanoprecipitation method, was first described by Fessi et al. in 1989 and is a frequently applied method for the preparation of polymeric nanoparticles because it is a relatively fast process with low energy input [32–36]. Using this method, the formation of polymeric micelles relies on the rapid diffusion of the organic phase with dissolved polymer chains into the external aqueous phase, followed by polymer aggregation to yield colloidal particles as demonstrated by Duan et al. for the formation of pH-sensitive polysialic acid based polymeric micelles [37]. The extent of polymer partition can be qualitatively described by comparing both solubility parameter difference ($\Delta\delta_{solvent\text{-}water}$) and solvent-water interaction parameter ($\chi_{solvent\text{-}water}$) [38–40]. Table S3 shows that DMF, DMSO, and DMAc display lower $\Delta\delta_{solvent\text{-}water}$ values (between 31.0 and 32.5 MPa$^{1/2}$) than THF and acetone (35.7 and 35.8 MPa$^{1/2}$), which points to a high solvent-water affinity of the first mentioned solvents and thus facilitates rapid polymer partition into the aqueous phase leading to rapid precipitation and the formation of smaller micelles (i.e., Z_{ave} of micelles prepared using DMF ≈ DMSO ≈ DMAc < THF and acetone). Acetone, with a lower $\chi_{solvent\text{-}water}$ value (23.4) than THF (27.1), forced more rapid polymer partition into the aqueous phase, which in turn resulted in polymeric micelles with a smaller average size as measured by DLS.

The micellar sizes measured by TEM were 25–47% smaller than those determined by DLS (Fig. 1A). This can be explained as follows. First, TEM observes nanoparticles in the dry state where the p(HPMAm) shell is invisible to the electron beam without chemical staining, whereas DLS measures the hydrodynamic diameter of nanoparticles including the solvation layers [41]. Second, TEM is a number-based measurement, whereas DLS measures intensity distributions based on Brownian motion. The detected light-scattering intensity is proportional to the six power of a particle diameter and thus larger particles are overestimated [42].

Notably, TEM images indicate that micelles formed using DMF had a narrow polydispersity (Fig. 1B & C). Therefore, DMF was selected for further micelle preparation.

The effect of the composition of the aqueous medium on the micellar size was also investigated. As shown in Fig. 2, the micelles showed comparable sizes when they were prepared in saline solution (57 ± 3 and 58 ± 3 nm in 0.9% NaCl and PBS, respectively). Our previous paper showed that the p(HPMAm)$_{7.1k}$-b-p(HPMAm-Bz)$_{15.0k}$ micelles demonstrated good colloidal stability in PBS upon incubation for 48 h at 37 °C [25]. In the current study, the size of micelles prepared in water did not change once this dispersion was mixed with an equal volume of either

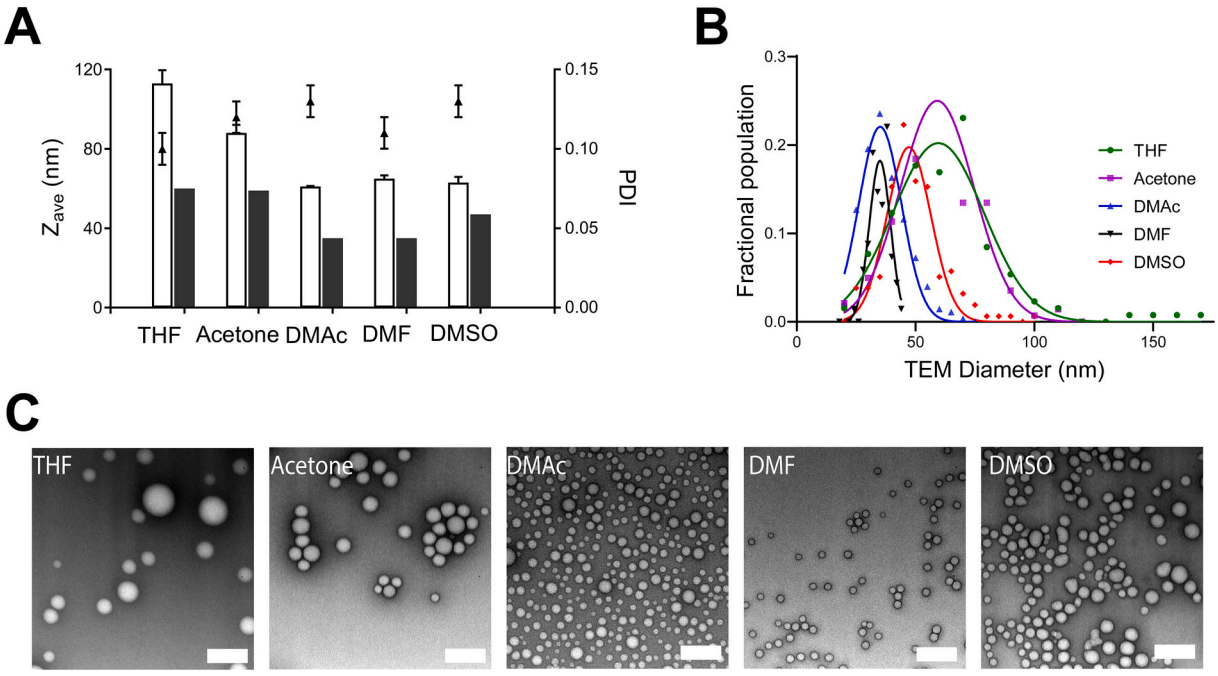

Fig. 1. Effect of organic solvent on micelle size. (**A**) Size of p(HPMAm)$_{7.1k}$-b-p(HPMAm-Bz)$_{15.0k}$ micelles prepared using different organic solvents, as determined by DLS (empty bars, $n = 3$) and TEM (filled bars, $n = 1$), and PDI (black dots, n = 3). (**B**) Size distribution of micelles as derived from TEM images. The curves of TEM diameter are the fitted Gaussian distributions. (**C**) TEM images of p(HPMAm)$_{7.1k}$-b-p(HPMAm-Bz)$_{15.0k}$ micelles prepared by using THF, acetone, DMAc, DMF, and DMSO as polymer solvent (from left to right). Scale bar represents 200 nm.

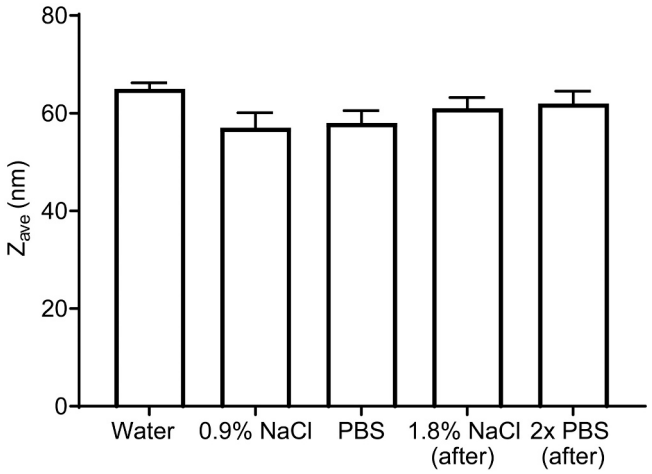

Fig. 2. Effect of aqueous medium on the size of p(HPMAm)$_{7.1k}$-b-p(HPMAm-Bz)$_{15.0k}$ micelles. Bars indicated with '1.8% NaCl (after)' and '2× PBS (after)' were micelle samples prepared in water and subsequently concentrated salt buffers were added ($n = 3$).

1.8% NaCl solution or twice concentrated PBS, making the resulted dispersions because of their osmotic values in principle suitable for intravenous injection, demonstrating that the micellar structures are thermodynamically stable.

3.2. Effect of the polymer concentration in DMF on the size of all-p(HPMAm) micelles

DMF solutions of p(HPMAm)$_{7.1k}$-b-p(HPMAm-Bz)$_{15.0k}$ with various concentrations were used for the preparation of micelles. As depicted in Fig. 3A, polymer concentrations from 5 to 40 mg/mL resulted in the formation of micelles in a range of 43 ± 2 to 73 ± 4 nm (PDI < 0.2). A similar phenomenon was observed for the formation of pH-sensitive micelles based on zwitterionic sulfobetaines prepared via solvent extraction method, where the average diameter of micelles increased from 70 to 110 nm when the concentration of poly(Ɛ-caprolactone)-b-poly-(*N*,*N*-diethylaminoethyl methacrylate)-r-poly(*N*-(3-sulfopropyl)-*N*-methacryloxyethy-*N*,*N*-diethylammoniumbetaine) increased from 1 to 10 mg/mL [43]. Likely, the increase of the polymer concentration in the organic solvent slows down the diffusion of the polymer-solvent into the aqueous solution due to the increased viscosity of the organic solution, leading to larger particles [35,36,44]. Our results indicate that this explanation is also valid for the all-HPMA based polymeric micelles investigated in the present study. However, different from the positive correlation between polymer concentration in DMF with micellar size of p(HPMAm)-b-p(HPMAm-Bz), in an earlier study we reported that the size of mPEG-b-p(HPMAm-Bz) micelles decreased with increasing polymer concentration up to 30 mg/mL in THF [45]. The discrepancy with the present study can be attributed to different polymer-organic solvent interactions, which needs further investigation.

3.3. Effect of organic/aqueous solvent ratio and the order of solvent addition on the size of all-p(HPMAm) micelles

The effects of the volume ratio of organic to aqueous solvent as well as the order of solvent addition on the size of the formed micelles were investigated. When the ratio of organic solvent to water was reduced from 1:1 to 0.3:1 using less DMF (1 and 0.3 mL) to dissolve the same amount of polymer, p(HPMAm)$_{7.1k}$-b-p(HPMAm-Bz)$_{15.0k}$ micelles with average sizes of 65 ± 1 and 87 ± 3 nm were formed by adding DMF to water, respectively (Fig. 3B). When water was added to DMF at 1:1 and 0.3:1 DMF/water volume ratios, the size of the resulting micelles was 90 ± 2 and 115 ± 2 nm, respectively. Regardless of the order of solvent addition, the reduction in the DMF/water ratio from 1:1 to 0.3:1 resulted in a significant increase in the average size of self-assembled micelles. Lower solvent-to-water ratio increased the initial weight fraction of polymer in organic solvent, i.e., polymer concentration increased from 20 to 67 mg/mL. It appears that these concentrations were below the critical overlap concentration (C* = 133 mg/mL), demonstrating that polymer chain entanglement did not occur and that this cannot explain the observations. The formation of larger particles might be therefore attributed to the increased viscosity of the organic solution with increasing initial weight fraction of the polymer, which subsequently retards diffusion of the polymer into the aqueous medium.

3.4. Effect of mixing time of organic and aqueous solvent on the size of all-p(HPMAm) micelles

Most of polymeric micelles aimed for cancer drugs are fabricated using bulk mixing methods leading to a lack of uniformity and reproducibility, which obstacles the translation to the industrial scales. Microfluidics provides precise control over the fluid flows and mixing time [46–48]. Therefore, the effect of mixing time of the organic and aqueous solvent on the size of the formed micelles was investigated using this technology. Photographs of p(HPMAm)$_{7.1k}$-b-p(HPMAm-Bz)$_{15.0k}$ micelle dispersions shown in Fig. 4A demonstrate that micellar dispersions obtained at higher total flow rate were opalescent, while those at lower flow rate were turbid. DLS measurements (Fig. 4B) evidenced that the micellar size increased from 52 ± 2 to 103 ± 3 nm (PDI

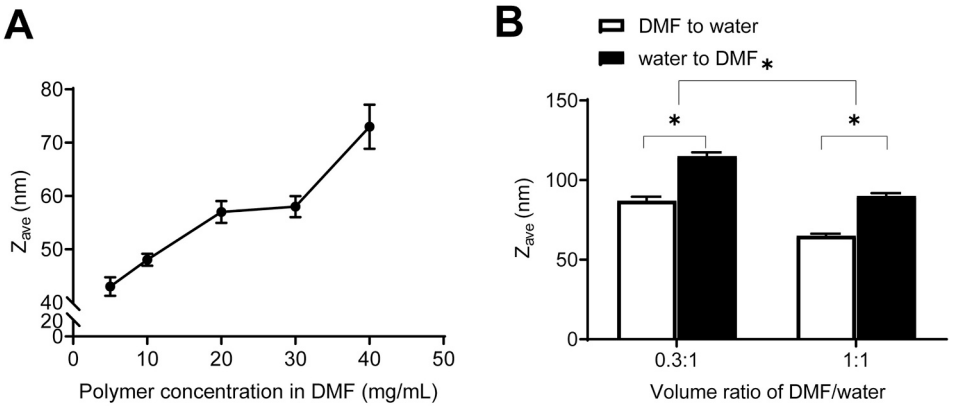

Fig. 3. Effect of polymer concentration and the order of solvent addition on micelle size. (**A**) Size of p(HPMAm)$_{7.1k}$-b-p(HPMAm-Bz)$_{15.0k}$ micelles as a function of the polymer concentration in DMF ($n = 3$). (**B**) The effect of DMF/water solvent ratio and the order of solvent addition on the size of p(HPMAm)$_{7.1k}$-b-p(HPMAm-Bz)$_{15.0k}$ micelles (n = 3). *p < 0.05.

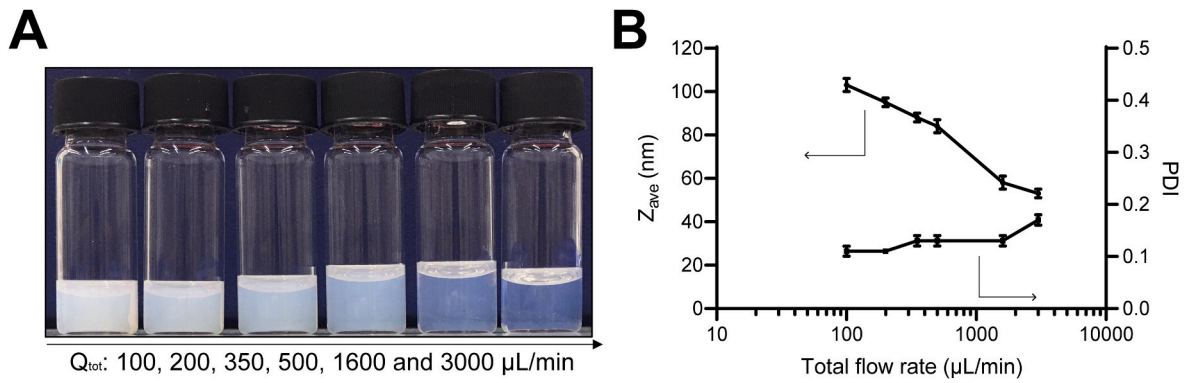

Fig. 4. Effect of mixing time of DMF and water on micelle size. (A) p(HPMAm)$_{7.1k}$-b-p(HPMAm-Bz)$_{15.0k}$ micelle dispersions obtained at different mixing times. (B) Size of p(HPMAm)$_{7.1k}$-b-p(HPMAm-Bz)$_{15.0k}$ micelles as a function of microfluidic flow rate (n = 3).

< 0.2) when the total flow rate decreased from 3000 to 100 μL/min (i.e., mixing time increased from 18 to 1571 ms). AF4-MALS analysis revealed that the aggregation number of the micelles (N_{agg}), calculated by dividing the weight-average molecular weight of micelles by the molar mass of a single polymer chain as determined by ^{1}H NMR, increased with increasing mixing time (Table 1). The ratio of radius of gyration and hydration (R_g/R_h), known as the shape factor, is 0.775 for rigid spheres with uniform density [49,50]. For particles composed of a dense core and a partly coiled less dense shell, the high concentration of the mass in the core leads to a small radius of gyration, and R_g/R_h values below the theoretical value of rigid spheres. For example, micelles with a dense spherical polystyrene core surrounded by a less dense poly (methacrylic acid) shell in a mixed solvent with dioxane and water (80:20 *v/v*), showed R_g/R_h values ranging from 0.37 to 0.64 [51]. It is also possible for a core-shell structure to have R_g/R_h > 0.775, as reported for core-shell spherical micelles based on cyclic poly(*N*-acryloylmorpholine)-grafted copolymer with R_g/R_h values ranging from 0.81 to 0.95 in water [52]. Table 1 shows that the resulting R_g/R_h values of the different micelles were between 0.53 and 0.66, which are slightly lower than that of rigid spheres, suggesting the formation of spherical micelles with a dense core and a swollen hydrated shell [53,54]. Similar results were observed for p(HPMAm)$_{7.1k}$-b-p(HPMAm-Bz)$_{9.1k}$ and p(HPMAm)$_{4.9k}$-b-p(HPMAm-Bz)$_{11.3k}$ (Fig. S3 & Table S4).

The flow rate dependence indicates that the formation of core-shell structured all-p(HPMAm) micelles is explained by the nucleation-controlled process. The addition of an anti-solvent (water) entails supersaturation, which in turn results in the nucleation and diffusion-limited growth of spherical aggregates with narrow distribution [55,56]. The rate of nucleation growth depends on the magnitude of supersaturation at a given temperature [46]. High flow rate results in fast mixing, and consequently the mixing time (τ_M) is approaching the aggregation time (τ_{agg}), inducing homogeneous local high supersaturation and rapid growth of spherical particles. This eventually results in numerous smaller micelles with narrow size distribution upon displacement of the organic solvent [48,57,58]. A similar phenomenon was also reported for the formation of mPEG-b-p(HPMAm-Bz) micelles using microfluidics [59]. These results demonstrate that the tunable mixing conditions significantly impacts the particle formation and growth kinetics and thus allows for the micelle preparation with a uniform size and size distribution. Continuous flow production ensures the same mixing quality over time, which in turn reduces batch-to-batch variation. For further scalable preparation of the all-HPMA based micelles, microfluidics is preferred over batch-mode production as it offers controlled size and features.

Table 1
Characteristics of p(HPMAm)-b-p(HPMAm-Bz) micelles obtained by microfluidics as determined by AF4-MALS.

Q_{tot} (μL/min)	τ_M (ms)	$M_{w,\ mic}$ (10^3 kDa)	N_{agg} (10^3)	R_g (nm)	R_h (nm)	R_g/R_h
100	1571	114	5.2	30	44	0.68
200	635	108	4.8	27	42	0.65
350	306	93	4.2	23	37	0.62
500	192	48	2.1	21	35	0.61
1600	42	16	0.7	15	25	0.59
3000	18	11	0.5	11	21	0.53

Q_{tot} = total flow rate, τ_M = mixing time, $M_{w,\ mic}$ = weight-average molecular weight of micelles determined by AF4-MALS, N_{agg} = the micelle aggregation number calculated by $M_{w,\ mic}/M_{n,\ p}$, where $M_{n,\ p}$ is the molar mass of a single polymer chain determined by ^{1}H NMR, R_g = radius of gyration, R_h = radius of hydration (n = 3, the standard deviation is less than 4%).

3.5. *Effect of p(HPMAm) and p(HPMAm-Bz) homopolymer presence on the size of all-p(HPMAm) micelles*

It has been reported the possibility of the presence of a small amount of homopolymer in block copolymers synthesized by RAFT polymerization [60–62], therefore, the effect of the presence of free homopolymer of p(HPMAm) and p(HPMAm-Bz) on the size of the formed p(HPMAm)-b-p(HPMAm-Bz) micelles was investigated by adding ~33% of p(HPMAm) or p(HPMAm-Bz) to the block copolymer solution. Fig. 5 shows that the size of p(HPMAm)$_{7.1k}$-b-p(HPMAm-Bz)$_{15.0k}$ micelles increased proportionally with increasing amount of homopolymer p(HPMAm-Bz)$_{14.6k}$ in DMF. This increase is because the hydrophobic p(HPMAm-Bz) is solubilized into the hydrophobic core, leading to an increase in the volume and thus diameter of the micelles. Fig. S4 presents similar results for p(HPMAm)$_{7.1k}$-b-p(HPMAm-Bz)$_{9.1k}$ and p

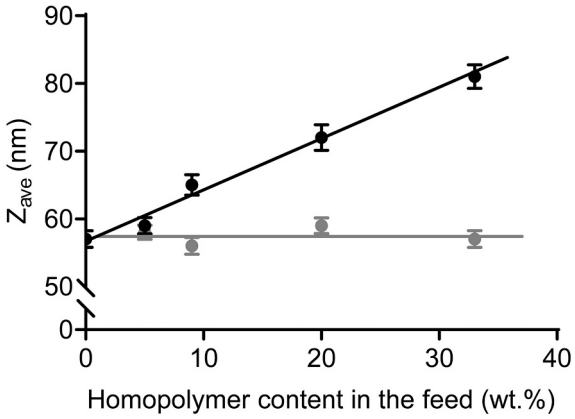

Fig. 5. Effect of the presence of free p(HPMAm)$_{7.1k}$ (gray) and p(HPMAm-Bz)$_{14.6k}$ (black) homopolymer in the feed dissolved in DMF on the size of p(HPMAm)$_{7.1k}$-b-p(HPMAm-Bz)$_{15.0k}$ micelles (n = 3).

$(HPMAm)_{7.1k}$-b-$p(HPMAm\text{-}Bz)_{4.9k}$ upon addition of $p(HPMAm\text{-}Bz)_{9.2k}$ and $p(HPMAm\text{-}Bz)_{4.7k}$, respectively. In contrast, the presence of the hydrophilic $p(HPMAm)_{7.1k}$ in the feed did not cause changes in micellar sizes (Fig. 5 & Fig. S4), which is ascribed to the good aqueous solubility of p(HPMAm) resulting in its partition in the aqueous phase. This is in agreement with the findings previously reported [45], in which the homopolymer p(HPMAm-Bz) led to an increase of mPEG-p-p(HPMAm-Bz) micelle, whereas the presence of up to 40% of free mPEG did not affect the micelle size.

3.6. Effect of hydrophilic/hydrophobic molecular weight of copolymers on the size of all-p(HPMAm) micelles

As there is no single, absolute method to characterize nanoparticles, especially in terms of morphology [63,64], to gain more insight into the impact of hydrophilic/hydrophobic molecular weight on micellar morphology, the block copolymers at fixed molecular weight of p(HPMAm) were used for the formation of micelles using batch process and further characterized by AF4-MALS, ultracentrifugation and Cryo-TEM.

Different from DLS measurements, AF4-MALS exploits the advantages of field-flow fractionation chromatography to separate fractions of nearly monodisperse self-assemblies with the power of multi-angle laser light scattering to get insight into their morphologies [65]. Table 2 shows that for micelles with a fixed hydrophilic p(HPMAm) block length, $M_{w,\,mic}$ and N_{agg} increased with increasing molecular weight of the hydrophobic p(HPMAm-Bz) block. For all polymeric micelles, the R_g/R_h values varied from 0.40–0.90, which was in the same range as reported for other core-shell structured micelles [54,66–68]. The surface area available per p(HPMAm) chain ($\boldsymbol{\sigma}^{-1}$), calculated by dividing the surface area of micelles by N_{agg}, was between 3 and 10 nm^2. The small surface area per p(HPMAm) chain (i.e., high grafting density) is a favorable property for drug delivery purposes as it has been reported that, for nanoparticles of equal size, an increasing PEG grafting density reduces adsorption of plasma proteins and thus prolongs blood circulation times [14,17]. The same might be expected for the all-HPMA based micelles. For block copolymers with a fixed molecular weight of the p(HPMAm) block, despite of the increased R_h and N_{agg} with increasing p(HPMAm-Bz) block length, the space between p(HPMAm) chains remained approximately the same (1.9 ± 0.1 nm for $p(HPMAm)_{3.0k}$, 2.5 ± 0.1 nm for p(HP MAm)$_{4.9k}$, and 2.8 ± 0.3 nm for $p(HPMAm)_{7.1k}$, respectively).

The validity of the AF4-MALS data was confirmed by analyzing two selected samples (Table 3) by ultracentrifugation which is an established and validated technique to determine the molecular weight of synthetic polymers and colloidal particles [30,69]. First, the partial specific volume of micellar dispersion was determined from the linear regression of a density-concentration profile of the micelles [70,71]. The concentration profiles were analyzed with Sedfit to obtain weight-average molecular weight of the micelles. The derived $M_{w,\,mic}$ and the deduced N_{agg} of $p(HPMAm)_{4.9k}$-b-$p(HPMAm\text{-}Bz)_{11.3k}$ micelles from ultracentrifugation were 12×10^3 kDa and 0.7×10^3, respectively, which is in good agreement with those determined by AF4-MALS technique ($M_{w,\,mic} = 14 \times 10^3$ kDa and $N_{agg} = 0.8 \times 10^3$). The consistency of two techniques was also demonstrated by $p(HPMAm)_{3.0k}$-b-$p(HPMAm\text{-}Bz)_{15.6k}$ (Tables 2 & 3). The determined value of frictional ratio f/f_0, providing valuable information regarding the shape of particles, is nearly one for spherical particles [30,72]. The f/f_0 value of both micelles was slightly above one (1.1–1.2), pointing to spherical structures, as evidenced by AF4-MALS that the R_g/R_h value was 0.56–0.90.

Table 3
Charateristics of two selected p(HPMAm)-b-p(HPMAm-Bz) micelles as determined by ultracentrifugation.

Polymer	$\bar{v}$ (mL/g)	$M_{w,\,mic}$ (10^3 kDa)	N_{agg} (10^3)	f/f_0
$p(HPMAm)_{3.0k}$-b-$p(HPMAm\text{-}Bz)_{15.6k}$	0.797	71	3.8	1.19
$p(HPMAm)_{4.9k}$-b-$p(HPMAm\text{-}Bz)_{11.3k}$	0.785	12	0.7	1.17

$\bar{v}$ = partial specific volume calculated by $1/\boldsymbol{\rho}$, where $\boldsymbol{\rho}$ is density of micelle dispersion determined by density meter, $M_{w,\,mic}$ = weight-average molecular weight of micelles determined by ultracentrifugation, N_{agg} = the micelle aggregation number calculated by $M_{w,\,mic}/M_{n,\,p}$, where $M_{n,\,p}$ is the molar mass of a single polymer chain obtained by ^{1}H NMR, f/f_0 = frictionl ratio (n = 3, the standard deviation is less than 5%).

To corroborate AF4-MALS and ultracentrifugation analyses regarding the morphology of samples, the selected micelle dispersions were further analyzed using Cryo-TEM. In line with AF4-MALS and ultracentrifugation data, both of $p(HPMAm)_{3.0k}$-b-$p(HPMAm\text{-}Bz)_{15.6k}$ and $p(HPMAm)_{4.9k}$-b-$p(HPMAm\text{-}Bz)_{11.3k}$ micelles showed spherical structures (Fig. 6). The average size as measured by Cryo-TEM was smaller than those of DLS (Table S6), which is indicative of partially coiled less dense shell making it invisible to the electron beam under Cryo-TEM.

The EPR effect as investigated and described by prof. Maeda in many papers is a hallmark in nanomedicine research as well as for the development of preclinical/clinical nanomedicine formulations. The size of nanomedicine is a crucial physicochemical factor for EPR-based drug delivery and targeting systems, and it has been reported that nanoparticles ranging from 10 to 150 nm are able to reach tumor sites through passive targeting after intravenous administration provided that these particles show sufficiently long circulating kinetics. Once accumulated in the tumor, size is also an important factor affecting tumor penetration of nanomedicines, and as general rule: the smaller the better. In the present study, several critical parameters that influence the size of all-HPMAm based micelles were investigated and discussed. In a nutshell, smaller micelles can be obtained by either proper selection of the organic solvent for the amphiphilic p(HPMAm)-b-p(HPMAm-Bz)

Table 2
Characteristics of p(HPMAm)-b-p(HPMAm-Bz) micelles as determined by AF4-MALS.

Polymer	dn/dc (mL/g)	$M_{w,\,mic}$ (10^3 kDa)	N_{agg} (10^3)	R_g (nm)	R_h (nm)	R_g/R_h	σ^{-1} (nm^2)	d (nm)
$p(HPMAm)_{3.0k}$-b-$p(HPMAm\text{-}Bz)_{5.4k}$	0.169	10	1.2	10	19	0.54	3.69	1.9
$p(HPMAm)_{3.0k}$-b-$p(HPMAm\text{-}Bz)_{9.9k}$	0.193	33	2.5	17	26	0.67	3.33	1.8
$p(HPMAm)_{3.0k}$-b-$p(HPMAm\text{-}Bz)_{15.6k}$	0.216	68	3.6	30	33	0.90	3.74	1.9
$p(HPMAm)_{4.9k}$-b-$p(HPMAm\text{-}Bz)_{6.4k}$	0.151	7	0.6	8	17	0.45	6.05	2.5
$p(HPMAm)_{4.9k}$-b-$p(HPMAm\text{-}Bz)_{11.3k}$	0.179	14	0.8	12	21	0.56	6.32	2.5
$p(HPMAm)_{4.9k}$-b-$p(HPMAm\text{-}Bz)_{16.8k}$	0.201	25	1.1	16	23	0.70	5.99	2.4
$p(HPMAm)_{7.1k}$-b-$p(HPMAm\text{-}Bz)_{4.9k}$	0.163	4	0.3	7	16	0.40	9.51	3.1
$p(HPMAm)_{7.1k}$-b-$p(HPMAm\text{-}Bz)_{9.1k}$	0.180	12	0.7	11	21	0.54	7.86	2.8
$p(HPMAm)_{7.1k}$-b-$p(HPMAm\text{-}Bz)_{15.0k}$	0.194	19	0.8	12	21	0.58	6.31	2.5

dn/dc = refractive index increment of the polymer determined by AF4, $M_{w,\,mic}$ = weight-average molecular weight of micelles determined by AF4-MALS, N_{agg} = the micelle aggregation number calculated by $M_{w,\,mic}/M_{n,\,p}$, where $M_{n,\,p}$ is the molar mass of a single polymer chain determined by ^{1}H NMR, R_g = radius of gyration, R_h = radius of hydration, σ^{-1} = surface area per p(HPMAm) chain calculated by $4\pi R_h^2/N_{agg}$, d = interchain distance calculated by the root square of σ^{-1} (n = 3, the standard deviation is less than 4%).

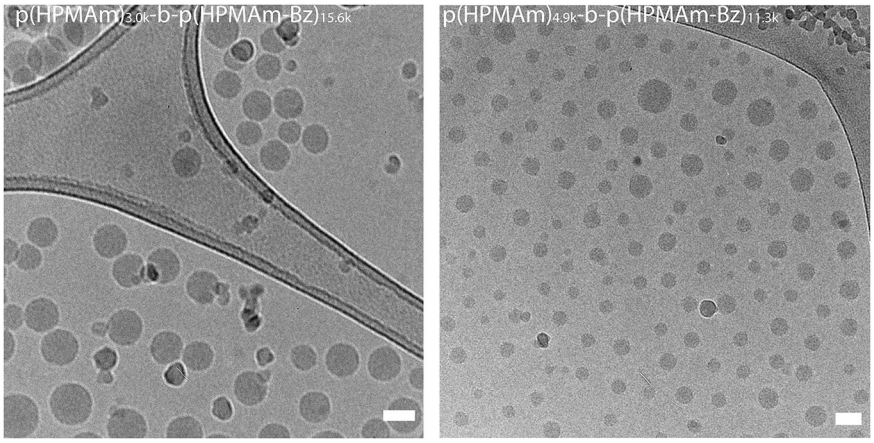

Fig. 6. Cryo-TEM images of micelles prepared from $p(HPMAm)_{3.0k}$-b-$p(HPMAm\text{-}Bz)_{15.6k}$ (left) and $p(HPMAm)_{4.9k}$-b-$p(HPMAm\text{-}Bz)_{11.3k}$ (right). Scale bar represents 50 nm.

block copolymer with faster mixing with water via microfluidics, or by using well-defined block copolymers with higher hydrophilic/hydrophobic ratios. A robust method was established to produce micelles in the size range of 40 to 120 nm, which can be exploited for EPR-driven tumor targeting.

4. Conclusion

This systematic study demonstrates that the self-assembly of p(HPMAm)-b-p(HPMAm-Bz) block copolymers into micelles can be tailored in size by solvent extraction method. The size control relies on the polymer hydrophobicity and hydrophilicity as well as processing method. It is important to take these parameters into consideration in practical applications of micelles.

Declaration of Competing Interest

There are no conflicts to declare.

Acknowledgements

The research was partially supported by the China Scholarship Council. The authors would like to thank Johanna Walther for her technical support in the application of microfluidics.

Appendix A. Supplementary data

Supplementary data to this article can be found online at https://doi.org/10.1016/j.jconrel.2022.01.042.

References

[1] H. Cabral, K. Miyata, K. Osada, K. Kataoka, Block copolymer micelles in nanomedicine applications, Chem. Rev. 118 (2018) 6844–6892.
[2] S. Eetezadi, S.N. Ekdawi, C. Allen, The challenges facing block copolymer micelles for cancer therapy: in vivo barriers and clinical translation, Adv. Drug Deliv. Rev. 91 (2015) 7–22.
[3] L. Houdaihed, J.C. Evans, C. Allen, Overcoming the road blocks: advancement of block copolymer micelles for cancer therapy in the clinic, Mol. Pharm. 14 (2017) 2503–2517.
[4] J. Kopeček, J. Yang, Polymer nanomedicines, Adv. Drug Deliv. Rev. 156 (2020) 40–64.
[5] R. Van Der Meel, E. Sulheim, Y. Shi, F. Kiessling, W.J.M. Mulder, Smart cancer nanomedicine, Nat. Nanotechnol. 14 (2019) 1007–1017.
[6] Y. Hussein, M. Youssry, Polymeric micelles of biodegradable diblock copolymers: enhanced encapsulation of hydrophobic drugs, Materials (Basel). 11 (2018), e11050688.
[7] A. Varela-Moreira, Y. Shi, M.H.A.M. Fens, T. Lammers, W.E. Hennink, R. M. Schiffelers, Clinical application of polymeric micelles for the treatment of cancer, Mater. Chem. Front. 1 (2017) 1485–1501.
[8] M. Talelli, C.J.F. Rijcken, C.F. van Nostrum, G. Storm, W.E. Hennink, Micelles based on HPMA copolymers, Adv. Drug Deliv. Rev. 62 (2010) 231–239.
[9] C. Deng, Y. Jiang, R. Cheng, F. Meng, Z. Zhong, Biodegradable polymeric micelles for targeted and controlled anticancer drug delivery: promises, progress and prospects, Nano Today 7 (2012) 467–480.
[10] K. Knop, R. Hoogenboom, D. Fischer, U.S. Schubert, Poly(ethylene glycol) in drug delivery: pros and cons as well as potential alternatives, Angew. Chem. Int. Ed. 49 (2010) 6288–6308.
[11] J. Fang, W. Islam, H. Maeda, Exploiting the dynamics of the EPR effect and strategies to improve the therapeutic effects of nanomedicines by using EPR effect enhancers, Adv. Drug Deliv. Rev. 157 (2020) 142–160.
[12] H. Maeda, J. Wu, T. Sawa, Y. Matsumura, K. Hori, Tumor vascular permeability and the EPR effect in macromolecular therapeutics: a review, J. Control. Release 65 (2000) 271–284.
[13] H.S. Min, H.J. Kim, J. Ahn, M. Naito, K. Hayashi, K. Toh, B.S. Kim, Y. Matsumura, I. C. Kwon, K. Miyata, K. Kataoka, Tuned density of anti-tissue factor antibody fragment onto siRNA-loaded polyion complex micelles for optimizing targetability into pancreatic cancer cells, Biomacromolecules. 19 (2018) 2320–2329.
[14] H. Zhou, Z. Fan, P.Y. Li, J. Deng, D.C. Arhontoulis, C.Y. Li, W.B. Bowne, H. Cheng, Dense and dynamic polyethylene glycol shells cloak nanoparticles from uptake by liver endothelial cells for long blood circulation, ACS Nano 12 (2018) 10130–10141.
[15] W. Huang, C. Zhang, Tuning the size of poly(lactic-co-glycolic acid) (PLGA) nanoparticles fabricated by nanoprecipitation, Biotechnol. J. 13 (2018), e1700203.
[16] M. Najafi, N. Kordalivand, M.A. Moradi, J. Van Den Dikkenberg, R. Fokkink, H. Friedrich, N.A.J.M. Sommerdijk, M. Hembury, T. Vermonden, Native chemical ligation for cross-linking of flower-like micelles, Biomacromolecules. 19 (2018) 3766–3775.
[17] C.D. Walkey, J.B. Olsen, H. Guo, A. Emili, W.C.W. Chan, Nanoparticle size and surface chemistry determine serum protein adsorption and macrophage uptake, J. Am. Chem. Soc. 134 (2012) 2139–2147.
[18] D. Hwang, J.D. Ramsey, A.V. Kabanov, Polymeric micelles for the delivery of poorly soluble drugs: from nanoformulation to clinical approval, Adv. Drug Deliv. Rev. 156 (2020) 80–118.
[19] J. Wang, W. Mao, L.L. Lock, J. Tang, M. Sui, W. Sun, H. Cui, D. Xu, Y. Shen, The role of micelle size in tumor accumulation, penetration, and treatment, ACS Nano 9 (2015) 7195–7206.
[20] H. Cabral, Y. Matsumoto, K. Mizuno, Q. Chen, M. Murakami, M. Kimura, Y. Terada, M.R. Kano, K. Miyazono, M. Uesaka, N. Nishiyama, K. Kataoka, Accumulation of sub-100 nm polymeric micelles in poorly permeable tumours depends on size, Nat. Nanotechnol. 6 (2011) 815–823.
[21] K. Huang, H. Ma, J. Liu, S. Huo, A. Kumar, T. Wei, X. Zhang, S. Jin, Y. Gan, P. C. Wang, S. He, X. Zhang, X.J. Liang, Size-dependent localization and penetration of ultrasmall gold nanoparticles in cancer cells, multicellular spheroids, and tumors in vivo, ACS Nano 6 (2012) 4483–4493.
[22] Y. Wang, Z. Wang, C. Xu, H. Tian, X. Chen, A disassembling strategy overcomes the EPR effect and renal clearance dilemma of the multifunctional theranostic nanoparticles for cancer therapy, Biomaterials. 197 (2019) 284–293.
[23] H. Soo Choi, W. Liu, P. Misra, E. Tanaka, J.P. Zimmer, B. Itty Ipe, M.G. Bawendi, J. V. Frangioni, Renal clearance of quantum dots, Nat. Biotechnol. 25 (2007) 1165–1170.
[24] H. Maeda, The 35th anniversary of the discovery of EPR effect: a new wave of nanomedicines for tumor-targeted drug delivery—personal remarks and future prospects, J. Pers. Med. 11 (2021), e229.
[25] Y. Wang, M.J. van Steenbergen, N. Beztsinna, Y. Shi, T. Lammers, C.F. van Nostrum, W.E. Hennink, Biotin-decorated all-HPMA polymeric micelles for paclitaxel delivery, J. Control. Release 328 (2020) 970–984.
[26] S.G. Weissberg, R. Simba, S. Rothman, Viscosity of dilute to moderately concentrated polymer solutions, Polymer (Guildf). 47 (1951) 298–314.

[27] M.L. Huggins, The viscosity of dilute solutions of long-chain molecules. IV. Dependence on concentration, J. Am. Chem. Soc. 64 (1942) 2716–2718.
[28] Y. Shi, R. Van Der Meel, B. Theek, E. Oude Blenke, E.H.E. Pieters, M.H.A.M. Fens, J. Ehling, R.M. Schiffelers, G. Storm, C.F. Van Nostrum, T. Lammers, W.E. Hennink, Complete regression of xenograft tumors upon targeted delivery of paclitaxel via Π-Π stacking stabilized polymeric micelles, ACS Nano 9 (2015) 3740–3752.
[29] M. Andersson, B. Wittgren, K.G. Wahlund, Accuracy in multiangle light scattering measurements for molar mass and radius estimations, Anal. Chem. 75 (2003) 4279–4291.
[30] P. Schuck, Size-distribution analysis of macromolecules by sedimentation velocity ultracentrifugation and Lamm equation modeling, Biophys. J. 78 (2000) 1606–1619.
[31] International Community of Harmonization (ICH), Impurities: guideline for residual solvents Q3C (R6), in: Int. Conf. Harmon. Tech. Requir. Regist. Pharm. Hum. Use 44, 2011, pp. 1–29.
[32] H. Fessi, F. Puisieux, J.P. Devissaguet, N. Ammoury, S. Benita, Nanocapsule formation by interfacial polymer deposition following solvent displacement, Int. J. Pharm. 55 (1989) 1–4.
[33] T. Jung, A. Breitenbach, T. Kissel, Sulfobutylated poly(vinyl alcohol)-graft-poly (lactide-co-glycolide)s facilitate the preparation of small negatively charged biodegradable nanospheres, J. Control. Release 67 (2000) 157–169.
[34] M. Beck-Broichsitter, J. Nicolas, P. Couvreur, Solvent selection causes remarkable shifts of the "ouzo region" for poly(lactide-co-glycolide) nanoparticles prepared by nanoprecipitation, Nanoscale. 7 (2015) 9215–9221.
[35] S. Galindo-Rodriguez, E. Allémann, H. Fessi, E. Doelker, Physicochemical parameters associated with nanoparticle formation in the salting-out, emulsification-diffusion, and nanoprecipitation methods, Pharm. Res. 21 (2004) 1428–1439.
[36] C.E. Mora-Huertas, H. Fessi, A. Elaissari, Influence of process and formulation parameters on the formation of submicron particles by solvent displacement and emulsification-diffusion methods: critical comparison, Adv. Colloid Interf. Sci. 163 (2011) 90–122.
[37] W. Zhang, D. Dong, P. Li, D. Wang, H. Mu, H. Niu, J. Duan, Novel pH-sensitive polysialic acid based polymeric micelles for triggered intracellular release of hydrophobic drug, Carbohydr. Polym. 139 (2016) 75–81.
[38] U. Bilati, E. Allémann, E. Doelker, Development of a nanoprecipitation method intended for the entrapment of hydrophilic drugs into nanoparticles, Eur. J. Pharm. Sci. 24 (2005) 67–75.
[39] A. Martin, P. Bustamante, A.H.C. Chun, Physical Pharmacy, 4th ed, Waverly International, 1993.
[40] C.M. Hansen, Hansen Solubility Parameters: A user's Handbook, 2nd ed., CRC Press, 2007.
[41] H. He, Y. Ren, Z. Wang, Z. Xie, A pH-responsive poly(ether amine) micelle with hollow structure for controllable drug release, RSC Adv. 6 (2016) 91940–91948.
[42] H. Hinterwirth, S.K. Wiedmer, M. Moilanen, A. Lehner, G. Allmaier, T. Waitz, W. Lindner, M. Lämmerhofer, Comparative method evaluation for size and size-distribution analysis of gold nanoparticles, J. Sep. Sci. 36 (2013) 2952–2961.
[43] X. Xie, Y. Ma, L. Huang, M. Cai, Y. Chen, X. Luo, Effect factors of micelle preparation for a pH-sensitive copolymer containing zwitterionic sulfobetaines, Colloids Surf. A Physicochem. Eng. Asp. 468 (2015) 31–39.
[44] M. Beck-Broichsitter, E. Rytting, T. Lebhardt, X. Wang, T. Kissel, Preparation of nanoparticles by solvent displacement for drug delivery: a shift in the "ouzo region" upon drug loading, Eur. J. Pharm. Sci. 41 (2010) 244–253.
[45] M. Bagheri, J. Bresseleers, A. Varela Moreira, O. Sandre, S.A. Meeuwissen, R. M. Schiffelers, J.M. Metselaar, C.F. van Nostrum, J.C.M. van Hest, W.E. Hennink, The effect of formulation and processing parameters on the size of mPEG-b-p (HPMA-Bz) polymeric micelles, Langmuir. 34 (2018) 15495–15506.
[46] M.A. Tomeh, X. Zhao, Recent advances in microfluidics for the preparation of drug and gene delivery systems, Mol. Pharm. 17 (2020) 4421–4434.
[47] S. Rezvantalab, M. Keshavarz Moraveji, Microfluidic assisted synthesis of PLGA drug delivery systems, RSC Adv. 9 (2019) 2055–2072.
[48] R. Karnik, F. Gu, P. Basto, C. Cannizzaro, L. Dean, W. Kyei-Manu, R. Langer, O. C. Farokhzad, Microfluidic platform for controlled synthesis of polymeric nanoparticles, Nano Lett. 8 (2008) 2906–2912.
[49] D. Kunz, A. Thurn, W. Burchard, Dynamic light scattering from spherical particles, Colloid Polym. Sci. 261 (1983) 635–644.
[50] S. Ohno, K. Ishihara, S.I. Yusa, Formation of polyion complex (PIC) micelles and vesicles with anionic pH-responsive unimer micelles and cationic diblock copolymers in water, Langmuir. 32 (2016) 3945–3953.
[51] A. Qin, M. Tian, C. Ramireddy, S.E. Webber, P. Munk, Polystyrene-poly (methacrylic acid) block copolymer micelles, Macromolecules. 27 (1994) 120–126.
[52] R.J. Williams, A. Pitto-Barry, N. Kirby, A.P. Dove, R.K. O'Reilly, Cyclic graft copolymer unimolecular micelles: effects of cyclization on particle morphology and thermoresponsive behavior, Macromolecules. 49 (2016) 2802–2813.
[53] C. Ma, P. Pan, G. Shan, Y. Bao, M. Fujita, M. Maeda, Core-shell structure, biodegradation, and drug release behavior of poly(lactic acid)/poly(ethylene glycol) block copolymer micelles tuned by macromolecular stereostructure, Langmuir. 31 (2015) 1527–1536.
[54] V.T.A. Nguyen, M.-C. De Pauw-Gillet, O. Sandre, M. Gauthier, Biocompatible polyion complex micelles synthesized from arborescent polymers, Langmuir. 32 (2016) 13482–13492.
[55] S.M. D'Addio, R.K. Prud'homme, Controlling drug nanoparticle formation by rapid precipitation, Adv. Drug Deliv. Rev. 63 (2011) 417–426.
[56] D. Horn, J. Rieger, Organic nanoparticles in aqueous phase, Angew. Chem. 40 (2001) 4330–4361.
[57] B.K. Johnson, R.K. Prud'homme, Mechanism for rapid self-assembly of block copolymer nanoparticles, Phys. Rev. Lett. 91 (2003), e118302.
[58] E. Lepeltier, C. Bourgaux, P. Couvreur, Nanoprecipitation and the "ouzo effect": application to drug delivery devices, Adv. Drug Deliv. Rev. 71 (2014) 86–97.
[59] J. Bresseleers, M. Bagheri, C. Lebleu, S. Lecommandoux, O. Sandre, I.A.B. Pijpers, A.F. Mason, S. Meeuwissen, C.F. Van Nostrum, W.E. Hennink, J.C.M. van Hest, Tuning size and morphology of mPEG-b-p(HPMA-Bz) copolymer self-assemblies using microfluidics, Polymers (Basel). 12 (2020), e2572.
[60] P. Yang, P. Pageni, M.P. Kabir, T. Zhu, C. Tang, Metallocene-containing homopolymers and heterobimetallic block copolymers via photoinduced RAFT polymerization, ACS Macro Lett. 5 (2016) 1293–1300.
[61] J. Arredondo, P. Champagne, M.F. Cunningham, RAFT-mediated polymerisation of dialkylaminoethyl methacrylates in tert -butanol, Polym. Chem. 10 (2019) 1938–1946.
[62] M. Danial, S. Telwatte, D. Tyssen, A. Postma, S. Cosson, G. Tachedjian, G. Moad, A. Postma, Combination anti-HIV therapy: via tandem release of prodrugs from macromolecular carriers, Polym. Chem. 7 (2016) 7477–7487.
[63] S. Mourdikoudis, R.M. Pallares, N.T.K. Thanh, Characterization techniques for nanoparticles: comparison and complementarity upon studying nanoparticle properties, Nanoscale. 10 (2018) 12871–12934.
[64] M.M. Modena, B. Rühle, T.P. Burg, S. Wuttke, Nanoparticle characterization: what to measure? Adv. Mater. 31 (2019) 1–26.
[65] Y. Hu, R.M. Crist, J.D. Clogston, The utility of asymmetric flow field-flow fractionation for preclinical characterization of nanomedicines, Anal. Bioanal. Chem. 412 (2020) 425–438.
[66] C.J.F. Rijcken, T.F.J. Veldhuis, A. Ramzi, J.D. Meeldijk, C. van Nostrum, W. E. Hennink, Novel fast degradable thermosensitive polymeric micelles based on PEG-block-poly(N-(2-hydroxyethyl)methacrylamide-oligolactates), Biomacromolecules. 6 (2005) 2343–2351.
[67] S. Dai, P. Ravi, C.Y. Leong, K.C. Tam, L.H. Gan, Synthesis and aggregation behavior of amphiphilic block copolymers in aqueous solution: di- and triblock copolymers of poly(ethylene oxide) and poly(ethyl acrylate), Langmuir. 20 (2004) 1597–1604.
[68] L.T.T. Trinh, H.M.L. Lambermont-Thijs, U.S. Schubert, R. Hoogenboom, A. Kjøniksen, Thermoresponsive poly(2-oxazoline) block copolymers exhibiting two cloud points: complex multistep assembly behavior, Macromolecules. 45 (2012) 4337–4345.
[69] J.L. Cole, J.W. Lary, T.P. Moody, T.M. Laue, Analytical ultracentrifugation: sedimentation velocity and sedimentation equilibrium, Methods Cell Biol. 84 (2008) 143–179.
[70] M. Raşa, U.S. Schubert, Progress in the characterization of synthetic (supramolecular) polymers by analytical ultracentrifugation, Soft Matter 2 (2006) 561–572.
[71] T.M. Laue, W.F. Stafford, Modern applications of analytical ultracentrifugation, Annu. Rev. Biophys. Biomol. Struct. 28 (1999) 75–100.
[72] Z. Bedö, E. Berecz, I. Lakatos, Mass, size and shape of micelles formed in aqueous solutions of ethoxylated nonyl-phenols, Colloid Polym. Sci. 265 (1987) 715–722.